RF Coil Design for MRI Using a Genetic Algorithm

J. Rock Hadley[1], Cynthia M. Furse[2], and Dennis Parker[1]

[1]Utah Center for Advanced Imaging Research
[2]Electrical and Computer Engineering
University of Utah
50 S Campus Drive 3280 MEB
Salt Lake City, Utah 84112
cfurse@ece.utah.edu
www.ece.utah.edu/~cfurse

Abstract – In this work a Genetic Algorithm (GA) was used to optimize single and dual array Radio Frequency (RF) coils for imaging vasculature structures using Magnetic Resonance Imaging. Quasi-static equations were used to simulate sample noise and signal sensitivity profiles of the coil elements. Coil to sample and coil to coil interactions were taken into account, and the relative signal-to-noise ratio in the structure of interest was used as the cost function for the GA optimization.

Key words – Genetic Algorithm, Magnetic Resonance Imaging, phased array coils.

I. INTRODUCTION

Previous work has shown that substantial improvement in Magnetic Resonance (MR) image quality can be obtained using receiver coils that are specifically designed for the region of interest [1 - 46]. However, it is often difficult to fully optimize RF coils (eg. their sizes and positions) for specific objects or anatomies because of the complex nature of coil/sample and coil/coil interactions. Obtaining the exact geometric configuration that will optimize image quality over the region of interest is complicated. Also, the optimal geometric parameters can vary greatly depending on the sample volume or structure being imaged. There is a general rule that the coil diameter should be approximately equal to the depth of the voxel being imaged [38], but when that object is a large volume (such as the heart) or when the structure is a tortuous long and varies in depth like an artery, optimization is difficult. Many characteristics need to be taken into account when designing RF coils for specific anatomy such as object geometry (structure of interest, structure shape, and body surface geometry), coil coupling, coil sensitivity profile, interaction with the sample, relative positions of individual elements, patient comfort, parallel imaging factors, and image acquisition technique.

Stochastic optimization methods such as the genetic algorithm (GA) [47 - 49] are well suited for optimization problems of this nature, since they are able to find a global minimum when many local minima exist, they require no derivatives or gradients, and they are very flexible in their utility. Cost functions for GAs can be tailored to specific problems and can be implemented with other types of algorithms for accurate measurement or optimization purposes. GAs have previously been used to generate MRI related design parameters for various applications including split coil magnets, biplanar gradients, and some RF coil designs [50 - 55]. In this work, GA techniques are used to optimize coil parameters pertaining to single loop coil and phased array coil design for the purpose of imaging specific anatomic structures. The GA technique can provide optimum coil parameters including the number of coils in the array and the specific size and position of each element in the array for imaging the specific anatomy. The goal of this work is not to evaluate standard GA methods, as applied to RF coil design, nor to provide exact specifications for building application-specific coils. Rather the goal of this work is to show that the GA is well suited for optimizing coil design parameters and to define cost functions and methods to enable this optimization, allowing coil developers to assess trends and tradeoffs in relative signal-to-noise ratio (rSNR) during structure specific optimization.

II. THEORY

Genetic Algorithms

The genetic algorithm [47] is a search and optimization technique based on the concept of natural selection. This technique is particularly useful for optimization problems that have complicated cost functions with many local minima. GAs are also used in cases where it is difficult to formulate multiple derivatives of the cost function for use in algorithms such as the steepest descent algorithm. The GA computes a cost function for its individual

"chromosomes" or vectors of numbers that describe the optimization problem. The GA begins by computing the cost function for an initial population of chromosomes that are randomly chosen over the search space. The most favorable chromosomes are kept, and the worst chromosomes are discarded. Those chromosomes that are kept are "mated" with other "good" chromosomes to form "offspring" chromosomes that are then put into the population pool. There are multiple techniques for mating chromosomes and introducing mutations into the chromosome pool so that the GA is less likely to result in a local minimum when the global minimum is desired. Although there is no way to determine if the absolute global minimum has been obtained, GAs are typically more likely to find the global minimum for cost functions containing many local minima than standard minimum seeking algorithms.

Optimization Model

The model for these simulations consists of a large slab (80 cm × 80 cm × 40 cm) of a semi-conducting material with coils placed on the surface of the conducting model [38]. The slab is defined for (-40 < x < 40, -40 < y < 40, -40 < z < 0), and the coils are placed on the surface of the slab at z = 0 as shown in Fig. 1. The y-axis of the slab is defined to be parallel to the main DC magnetic field of the MR scanner, B_0. The sample has a conductivity of 0.3 S/m. Off-axis electromagnetic equations for rectangular coil elements are simulated using equations derived from the Biot-Savart law and presented by Smythe and Misakian [56], [57]. For a single loop, the dimensions are a × b, representing the side lengths of a rectangular coil in the x and y directions, respectively. The coil position is defined as (x, y) as shown in Fig. 1. The anatomic object of interest is embedded in the sample and consists of any collection of points that represent the particular structure over which rSNR calculations are made. The objects of interest in this work primarily consist of representations of different vessel structures and a heart shaped object.

The impedance, Z, for an RF resonating loop receiver coil is composed of several terms including the sample losses, R_s, coil ohmic losses, R_c, the connecting wire or cable losses R_w, the amplifier impedances, R_a, and the reactive inductance and capacitance terms, X,

$$Z_i = R_{si} + R_{ci} + R_{wi} + R_{ai} + jX_i. \tag{1}$$

The i represents the i^{th} coil, $j = \sqrt{-1}$. The sample noise R_s, for such a coil is defined as the integral of the squared magnitude of the magnetic vector potential, A, created by a unit current in the coil [58], multiplied by the sample conductivity, σ, and the squared radian frequency, ω, over the volume of the coil sensitivity [38], [56]

$$Rs_i = \omega^2 \sigma \int A_i \cdot A_i \partial v. \tag{2}$$

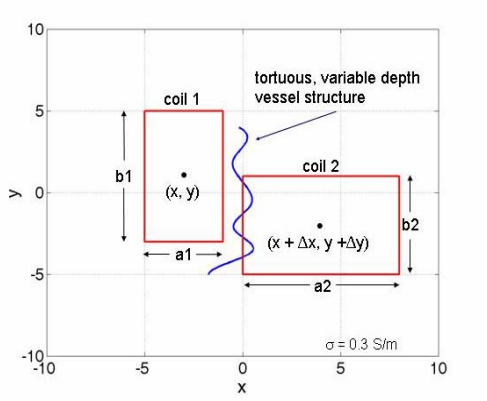

Fig. 1. Coil dimension and position definitions for a single and dual coil system positioned over the optimization sample space.

For this equation, it is assumed that the conductivity tensor is isotropic and uniform over the sample volume, and that only a ϕ component of the magnetic vector potential exists in the sample [56]. This satisfies the boundary conditions for the electric field at the sample boundary. The coil ohmic losses for the rectangular loop are [59]

$$Rc_i = \frac{4(a_i + b_i)}{\pi d}\sqrt{\frac{\mu_o 2\pi f}{2\sigma}}, \tag{3}$$

where μ_0 is the permeability of air, f is the frequency of the current in the conductor, and d is the diameter of the conductor. This work does not include the amplifier or cable losses based on the assumption that these losses are already minimized and are the same for all coils in the optimization algorithm. For a single loop, the reactive terms include the distributed capacitance and the loop self inductance terms that generally cancel out at resonant frequencies. However, the self inductance terms are useful in the coil optimization process. For a single rectangular loop coil of dimensions a × b, with a round wire diameter ρ, the self inductance is [60],

$$L_i = 0.004(a_i \log(2a_i/\rho) + b_i \log(2b_i/\rho) + 2\sqrt{a_i^2 + b_i^2}$$
$$-a_i \sinh^{-1}(a_i/b_i) - b_i \sinh^{-1}(b_i/a_i) - 2(a_i + b_i) + \frac{\mu}{4}(a_i + b_i)). \tag{4}$$

For the purposes of this work, the noise power, n, for a single coil is defined by equation (2) and equation (3) such that,

$$n_i = \mathrm{Re}\left(Z_i\right) \approx Rs_i + Rc_i. \tag{5}$$

The relative MR signal or coil sensitivity for a point in the sample space r is defined from the theory of reciprocity [58] as the transverse magnetic field produced by the coil with a unit current flowing in the conductor elements,

$$s_i(r) = B_\perp \approx (B_x(r) + jB_z(r)). \tag{6}$$

For a two coil system, the second rectangular loop has the dimensions of $a_2 \times b_2$, with a position of $(x + \Delta x, y + \Delta y)$ as depicted in Fig. 1. The second coil also has its own self inductance described by equation (4). There is also a mutual inductance term that describes the flux linkage between the two coils. This term is largely dependant on the geometrical relationship between the two coils and is expressed by,

$$M_{ik} = \frac{\mu_0}{4\pi} \iint \frac{\partial s_i \cdot \partial s_k}{|r_i - r_k|}, \tag{7}$$

where, s_i is a unit element of the conductor of coil i, and $|r_i - r_k|$ is the distance between the unit elements of the i^{th} and k^{th} coil.

The second coil also has sample noise and ohmic noise described by equations (2) and (3), respectively. If the two coils are in close proximity, a portion of the sample noise can be correlated between coils. This correlated noise power or noise that is shared between the two coils, through the sample, is described by,

$$Rs_{ik} = \omega^2 \sigma \int A_i \cdot A_k \partial v, \tag{8}$$

which is the general form of equation (2), including the inner vector product of the magnetic vector potential from both coils at each point in the sample space. These additional noise terms from coil k affect the noise of the overall system and the resulting noise as seen by coil i is,

$$n_{ti} = R_{si} + R_{ci} + \sum_{i \neq k} R_{ik} + \sum_{i \neq k} \left| \frac{\omega M_{ik}}{Z_k} \right|^2 \mathrm{Re}(Z_k^*), \tag{9}$$

where the subscript t represents the total noise from the i^{th} coil. The net signal or coil sensitivity for coil i, in the presence of coil k, then become,

$$s_i(r) = \left(Bx_i(r) + jBz_i(r)\right) + \sum_{i \neq k} \frac{M_{ik}}{L_i} \left(Bx_k(r) + jBz_k(r)\right). \tag{10}$$

The rSNR at any given point in the sample depends on combining the signals from coil i and coil k in the manner derived by Roemer [38]. Therefore, when the signals are combined to obtain maximized rSNR at every image point, the resulting maximum rSNR is,

$$rSNR = \sqrt{S^T \Psi^{-1} S^*}, \tag{11}$$

where S is the coil sensitivity vector, or the vector of coil sensitivities at the position for which the rSNR is being calculated. The T represents the matrix transpose, * represents the complex conjugate, and Ψ is the noise correlation matrix which includes the noise power terms from equation (2) as the diagonal elements, and the noise power terms from equation (8) as the off diagonal elements of its matrix.

III. METHODS

Genetic Algorithm

The GA chromosomes that describe the one and two coil systems consist of the geometrical parameters that express the sizes of the coils and their positions with respect to the sample being imaged (see Fig. 1). The chromosome for the two coil system is:

$$[a_1, b_1, x, y, a_2, b_2, \Delta x, \Delta y]. \tag{12}$$

For this work, these chromosome variables were continuous, although it would be equally valid to allow a fixed set of choices, which might speed up the GA convergence. The ranges for a and b define limitations on the smallest and largest coil sizes allowed in the optimization, and the limits on x, and y determined the limits of the coil position. The coils in this study are limited to a maximum a and b of 10 cm, and the center position of the search space is a 20 × 20 cm surface.

An initial set of 16 to 48 random chromosomes were compared based on their cost function values. The best half of the chromosomes were kept for mating (parents) and the rest of the chromosomes were discarded. The mating routine produced the same number of additional offspring chromosomes, which were sorted with the parent chromosomes according to their cost function values (their "fitness"). This iterative procedure was continued until convergence was achieved.

The cost function for each chromosome was computed as the average rSNR for the sample points in the object of interest,

$$\cos t = \frac{1}{N} \sum_{i=1}^{N} w_i \cdot rSNR(r_i). \tag{13}$$

For this equation, rSNR is defined by equation (11), r_i defines the position of the sample, point, N is the total number of sample points that define the anatomic structure of interest, and w_i is the weighting value of specific sample points ($w_i = 1$ for this work). For each rSNR calculation, the coil sample and ohmic losses were interpolated from pre-computed look up tables, eliminating the computation of time consuming volume

integrals over the sample space for each iteration. The coil signal sensitivity at all sample points was also computed for each coil, or set of coils, and for each GA iteration.

The original implementation of the two coil GA code used the equations as stated above to compute the cost functions of the chromosomes. However, the GA would quickly converge to local minimum solutions where the mutual inductance between coils was zero, but for which the coil shapes and positioning were not practical or intuitive for imaging the object of interest. Using continuous variables for the chromosome elements caused the solution space to be so large that it was difficult to find another local minima once the first set of $M_{12} = 0$ coils were determined. Consequently, the first local minimum found was generally the final result for this algorithm. These $M_{12} = 0$ solutions were very dominant over all other solutions and many such solutions (local minima) existed in the search space. Therefore, it was determined that the search space should be limited to solutions where the mutual inductance between coils was zero. This is commonly done in coil design without the GA, and it is reasonable to assume that it is also ideal for GA-optimized coils. This work used a simple binary search algorithm to shift coil 2, along a specified angle with respect to coil 1, to determine the Δx and Δy chromosome elements that would result in $M_{12} = 0$ between the two coils. Consequently, Δx and Δy can quickly be determined. Once this algorithm is complete, the Δx and Δy components of the two coil chromosome were set, and the relative position of coil 2 with respect to coil 1 was fixed. At that point, the correlated noise terms between the two coils were calculated, the individual coil sample noise terms were obtained from the lookup table, and the noise correlation matrix, Ψ, was defined for the two coil system. The binary search algorithm essentially eliminated two of the eight chromosome elements in the original 2 coil chromosomes. The next step that aided in significantly speeding up the algorithm, was the use of a nested GA to optimize the (x, y) position of coil 1 such that the average rSNR of the fixed two coil system was optimized for the object of interest. This nested GA was fast, because the only calculations needed for each iteration were the magnetic field and rSNR calculations for the object points at each (x, y) coil pair position. This technique resulted in a 4 element GA in an outer loop and a two element GA in an inner loop, and significantly reduced the chromosome pool search space to include only chromosomes that were relevant and practical for imaging the object of interest. This technique provides significant improvements in the speed of convergence over a single GA for all eight elements of the chromosome. Other factors that speed up convergence of the GA were to restrict the relative sizes of the two coils so that non-probable coil pairs were eliminated and the use of predetermined coil pair data that wais used in a look up table as the initial pool of chromosomes. All that wais needed for these initial chromosomes wais the inside GA loop to optimally position the coil pairs for imaging the object of interest. Finally, the option to fine tune the top chromosome wais included in the algorithm. This consists of adding chromosomes with incremental adjustments in the coil sizes and positions into the pool and helped to keep the GA from stagnating on a single chromosome for multiple iterations.

Coil Optimizations

Single coil GA simulations used a reduced chromosome length of 4 elements including the coil dimensions a and b, and the coil position x and y. Noise correlation and mutual inductance terms were not needed for these simulations, so convergence was quick. Single coil optimizations were performed to compare single and double coil rSNR results and to assess the relative improvements that can be gained by using two coils over a single coil for various vessel segments.

Several case studies were evaluated [79] and are discussed here. For each case a single and double coil GA optimization were performed. The case studies consisted of the following: case 1) a single sample point, representing a vessel segment of 1 cm length at a 3 cm depth, , case 2) a single sample point at 5 cm depth, case 3) a single sample point at 8 cm depth, case 4) a longer vessel segment of 4 cm length at a continuous depth of 3 cm, case 5) a longer vessel segment of 10 cm length at a 5 cm depth, case 6) a long vessel structure with a linear depth profile, with a length of approximately 11 cm, a depth of 2.5 cm at one end, a depth of 5 cm at the center and a depth of 7.5 cm at the deepest end, and case 7) a heart model consisting of approximately 300 points distributed on a stretched spheroidal surface with a center depth of 9 cm, a length of 10 cm, and a diameter of 7 cm.

IV. RESULTS

The results for all the single and dual coil optimizations for the various cases are presented in Table 1. This table shows that for a single vessel point at 3 cm depth, the optimal coil radius is approximately 1.9×1.9 cm, and as a consequence of the vessel point being positioned at (x, y, z) = (0, 0, -3) cm, the coil is positioned at (x, y) = (0, 0) cm. This is about 25 % different from the rule of thumb that the coil diameter should be 3 cm for a 3 cm deep voxel. The rSNR for this single point using the optimal single coil is 81.6.

For the same vessel point, using a two coil array, the dimensions of each coil were 1.6×2 cm with a 2.72 cm x-directed, patient left/right, or transverse offset

between the two coils. This is similar to the designs presented by Hayes where the coils are offset in the transverse direction for optimal rSNR [22], [23], [61]. This configuration of coils provided a 14.8 % improvement in the rSNR (93.7) over the single coil. Hayes has described this phenomenon and attributes this to the phase of the coil sensitivity profile at the point of interest [62]. Similarly for cases 2 and 3, the dual coil array provides similar rSNR improvement with coil elements offset in the transverse direction. These results also show the intrinsic rSNR loss that naturally occurs as the sample point increases in depth. For example, increasing the depth of the single sample point from 3 to 5 cm decreases the available rSNR using the two coil array by 65 %, and increasing the depth from 5 to 8 cm decreases the available rSNR by an additional 65 %.

Table 1. GA optimization results for case studies.

Case #	# coils	depth	length	a/2	b/2	x	y	rSNR	% chg
1. point	1	3	1	1.9	1.9	0	0	81.6	14.8
	2	3	1	1.6	2	-1.37	0	93.7	
				1.6	2	1.37	0		
2. point	1	5	1	2.7	2.7	0	0	27.9	15.1
	2	5	1	2.3	3	1.9	0.2	32.1	
				2.3	3	-1.9	-0.17		
3. point	1	8	1	4	4	0	0	9.8	15.3
	2	8	1	3.4	4.5	-2.84	-0.28	11.3	
				3.4	4.5	2.87	0.28		
4. vessel	1	3	4	1.8	2.5	0	0	71.1	17.4
	2	3	4	1.6	2.6	1.29	-0.21	83.5	
				1.6	2.6	-1.31	0.23		
5. vessel	1	5	10	2.5	5	0	0	20.6	26.2
	2	5	10	2.7	3.1	0.15	2.69	26	
				2.7	3.1	-0.15	-2.68		
6. vessel	1	2.5 – 7.5	11	2	3	0	2.7	29.7	26.3
	2	2.5 – 7.5	11	1.8	2	0	3.8	37.5	
				3	3.2	0	-0.6		
7. heart	1	9	10	4	6	0	0	6.7	23.9
	2	9	10	3.7	6.5	-3	0.29	8.3	
				3.7	6.5	3	-0.29		

For case 4, the vessel object is again at a 3 cm depth, and the length is increased to 4 cm, typical for a carotid bifurcation. For this case, use of a dual coil array provides approximately 17.4 % rSNR improvement over the single coil (see Fig. 2). It is also interesting to note that by optimizing coils over a larger volume or vessel length, there is a nearly 11 % reduction in available rSNR compared to a single point at the same depth (compare with case 1). This coil design might be considered to be a good coil design for applications where the object of interest is a single point somewhere along the artificial design vessel, and the goal of the coil design is to have improved flexibility in coil positioning for a tradeoff of nearly 11 % in rSNR.

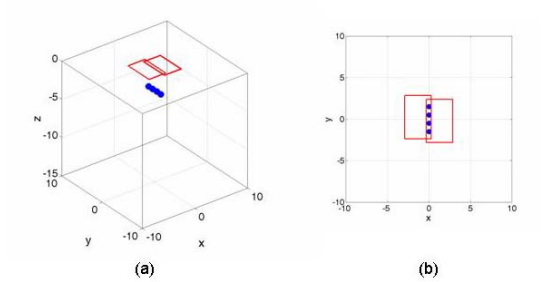

Fig. 2. Case 4 dual coil results show that the coils are still overlapped in the transverse direction and that there is a 17.4 % increase in rSNR compared to the single coil results.

The GA solution for case 5 indicates that the optimal dual coil configuration consists of two coils that are nearly the same size as an optimal single element coil for a single point at the design depth (see Fig. 3). However, rather than positioning the coils such that they are overlapped in the transverse direction, they are overlapped in the longitudinal direction, or patient superior/inferior direction. This configuration is known to have a subtle rSNR decrease under the overlap of the two coils as opposed to the known increase in rSNR under the overlap for coils overlapped in the transverse direction [62]. However, for the cost function used in this study, the net rSNR for the longitudinally overlapped pair is greater than for designs using the transverse overlapped pair. The GA technique can aid in determining where this break point might be found in determining the best approach for coil overlap for the imaging of specific structures. This case also demonstrates, as before, that designing a coil to cover such a long structure decreases the available rSNR of any one point on the structure by 19 % compared to a coil designed for a single point at the same depth (compare with case 2). However, this coil design is likely to be more flexible in positioning along the length of the structure.

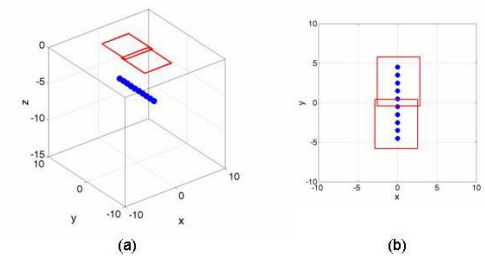

Fig. 3. Case 5: dual coil results show that the optimal overlap for this case is in the longitudinal direction. The dual coil provides a 26.2 % increase in rSNR over the single coil results.

The results for case 6 (see Fig. 4) give an indication of how the appropriate coil array should be designed to image structures that change in depth along the length of the structure. It would be difficult to use intuition alone to design a coil for such a purpose, however, using the GA to optimize the coils for this vessel structure provides a result that is intuitive and gives relative estimates of the dimensions and positions of a dual coil array that might be used to image a structure such as this. It is interesting to note how much rSNR improvement (~26 %) the GA indicates can be achieved using two coils rather than a single coil for these long vessel cases. This result also indicates that it may be important to use coils of arbitrary shape for the imaging of specific structures rather than standard circular or rectangular shaped coils.

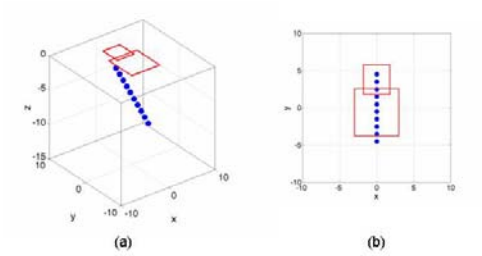

Fig. 4. Case 6: dual coil results show the benefit of using arbitrary shaped coils for imaging structures of this nature. The dual coil for this case provides a 26.3 % increase in rSNR compared to the single coil for this case.

The results for the heart model, case 7, provide insight into the optimal coil design for larger volumes and structures. The sample points used to calculate the average rSNR over the surface of this structure range from 12.5 cm to 5.5 cm depth with a slightly larger sample point density at the superior and inferior ends of the model, near its central axis (see Fig. 5). Because of the long length of this structure, it might be expected that coils overlapped in the longitudinal direction would again provide the highest rSNR over its surface. However, because the sample points nearest the surface have the largest intrinsic rSNR, their contribution to the overall cost function is great, and result in an optimal coil design where the coils are overlapped in a transverse manner with respect to B_0. Comparing case 7 with case 3, it can be seen that the coil width radius, a/2 = 3.7 cm, is just slightly larger than that for the single point at 8 cm depth, a/2 = 3.4 cm, accounting for the extra centimeter of the average heart depth. However, in order to account for the length of the heart at such a depth, the coil radius for the longitudinal direction is considerably longer than for the result in case 3. Finally, these results indicate an rSNR increase of approximately 24 % using a dual coil array compared to a single coil.

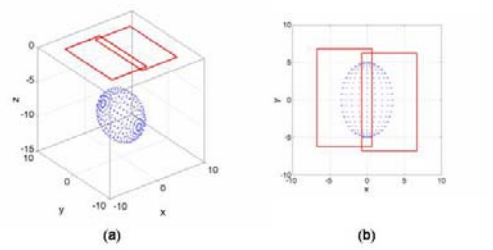

Fig. 5. Case 7: dual coil results show that, for the average rSNR cost function, the coils are still overlapped in the transverse direction even though the structure is long. The dual coil for this case provides a 23.9 % increase in rSNR over the single coil for this case.

The results for the single coil optimizations are in line with intuition and with expected results. Results for the single coil GA are achieved quickly, and can be performed on a standard PC in a matter of minutes. Using the techniques described above on a Dual AMD Opteron, dual core 270 with 4 GB of RAM, case 4 converged in approximately 2.5 hours, and case 7 in approximately 9.55 hours, making these simulations practical to use for specific design applications.

V. DISCUSSION

The purpose of this work was to develop a GA tool that could be used for finding coil geometries and positions that give the highest rSNR for a specific anatomy, and evaluate its usefulness. Modifications were made to the standard GA methods that limit the coil parameter search space to solutions that are practical for imaging the object of interest. Although these simulations were performed for only two coils, it would be natural to extend this work to multi-element arrays. There are challenges in obtaining minimum mutual inductance for three or more coil elements. However, with the use of passive decoupling circuits [28], [63 - 66] and appropriate image reconstruction techniques [65], [67], zero mutual inductance between all adjacent, coils may not be required. With the ability to simulate and optimize multiple coil elements using the GA tool, the number of coil elements that might be used in an array for imaging a specific structure might also be optimized.

In addition to optimizing the number of elements used in a coil array, many other interesting coil design characteristics might be optimized using the GA techniques such as individual coil sizes and relative positions for phased array coil elements, g-factors, and coil element spacing for parallel imaging applications, and any other coil dimension or relative coil position. Cost functions can also be modified to include other

anatomic structure specifications or image acquisition parameters. Recently, Breuer and Griswold have shown that phased array designs may be optimized for specific parallel image acquisition schemes that use different data gridding techniques. [68], [69] Therefore, the results of this study indicate that the use of the GA for optimization of coil design parameters is useful and promising.

The purpose simulating these different cases was to evaluate coil design trends and the effects on rSNR for different imaging applications, providing answers to fundamental coil design questions concerning coil size, position, direction of overlap, etc. These different case studies were also designed to provide insight into the results of designing RF coils for various objects of interest and to better understand how the optimal coil should be configured for these different geometries. It can be seen that coils or arrays of coils that are optimized for a specific point in the sample can provide significantly more rSNR for that point than if the point is only a part of some greater volume or structure that is being imaged with a coil designed for the entire volume.

There are several limitations to this study. First, particularly for complicated anatomies such as the carotid bifurcation, the simple vessel models may be insufficient. More realistic models would include accurate representation of the head, neck and shoulders and full wave solutions to account for all the complicated boundaries of such a model. Such a model would also provide the appropriate sample and correlated loss terms, whereas the infinite half plane model used in these studies may represent a much more dominant load than that of the head, neck and shoulders.

Second, these simulations are based on quasi-static electromagnetic field simulations where it is assumed that the electric and magnetic fields are not coupled and that the magnetic field in the sample is primarily due to the current in the coil conductor. Simulations using these equations combined with the effectively infinite slab model are subject to error, because they do not take into account important effects such as the boundary conditions of actual human anatomy, sample loading, conductive shielding of the fields from the sample, etc. Wright has computed the rSNR for several different coils at 64 MHz and has shown that the results using the quasi-static solutions tend to show all appropriate trends and features of the coils compared to actual measurements [44]. Many other authors have used quasi-static calculations to obtain reasonable estimates of real measurements [9], [20], [38], [56], [70-78]. These simulations seem to work well for situations where the current distributions around the coils are known to be relatively constant across the coil. As the coil dimensions or the frequency increases the changes in phase of the current in the coil become more significant, and these simulations may be inaccurate in predicting appropriate rSNR trends and characteristics.

Finally, it is also important to note that these simulation results are based on a cost function that is computed as the average rSNR over all sample points that define the structure of interest. The cost function also assumes the use of Roemer's full reconstruction algorithm (equation (11)) [38]. These results might be significantly different if the sample points were weighted to emphasize different sections of the structure or if different reconstruction algorithms were used to combine data from multiple coils.

VI. Conclusions

This work demonstrates that the GA can be used as a coil design tool to study rSNR characteristics for imaging applications of specific anatomic structures, where relative trends and tradeoffs of various coil configurations can be understood. Although GAs typically require large amounts of computing power, modifications can be made to decrease the parameter search space and improve the speed of RF coil GA optimizations. Cost functions for the GA coil optimization can be modified to include larger numbers of array elements as well as other interesting coil parameters such as g-factor and array element spacing for parallel imaging applications, as well as size, shape, and total number of elements in an array for optimal rSNR imaging.

The case studies presented in this work demonstrate important characteristics of various coil designs optimized to image specific anatomic structures, and provide answers to fundamental questions concerning the design of RF coils for MRI.

References

[1] M. Alecci, C. M. Collins, J. Wilson, W. Liu, M. B. Smith, and P. Jezzard, "Theoretical and experimental evaluation of detached endcaps for 3 T birdcage coils," *Magn. Reson. Med.,* vol. 49, no. 2, pp. 363 - 370, 2003.

[2] E. Atalar, P. A. Bottomley, O. Ocali, L. C. Correia, M. D. Kelemen, J. A. Lima, and E. A. Zerhouni, "High resolution intravascular MRI and MRS by using a catheter receiver coil," *Magn. Reson. Med*., vol. 36, no. 4, pp. 596 - 605, 1996.

[3] E. Atalar, P. A. Bottomley, and E. A. Zerhouni, *A Flexible Catheter Coil for Imaging and Spectroscopy of Atherosclerotic Plaques*, Nice, p. 988, 1995.

[4] L. Axel and C. Hayes, "Surface coil magnetic resonance imaging," *Arch. Inst. Physiol. Biochim.,* vol. 93, no. 5, pp. 11-18, 1985.

[5] F. Bernstein, G. Slavin, R. A. Day, F. Macaluso, and S. D. Wolff, *A Phased Array Coil Optimized for Carotid Artery Imaging*, Philadelphia, p. 163, 1999.

[6] D. Beyer, W. Steinbrich, G. Friedmann, and J. W. Ermers, "Use of surface coils in magnetic resonance imaging or orbit and knee," *Diagn. Imaging Clin. Med.,* vol. 55, no. 1-2, pp. 84 - 91, 1986.

[7] P. A. Bottomley, C. H. Lugo Olivieri, and R. Giaquinto, "What is the optimum phased array coil design for cardiac and torso magnetic resonance?," *Magn. Reson. Med*., vol. 37, no. 4, pp. 591 - 599, 1997.

[8] M. J. Chelsky, M. D. Schnall, E. J. Seidmon, and H. M. Pollack, "Use of endorectal surface coil magnetic resonance imaging for local staging of prostate cancer," *J. Urol,* vol. 150 (2 Pt 1), pp. 391 - 395, 1993.

[9] C. D. Constantinides, C. R. Westgate, W. G. O'Dell, E. A. Zerhouni, and E. R. McVeigh, "A phased array coil for human cardiac imaging," *Magn. Reson. Med.,* vol. 34, no. 1, pp. 92 - 98, 1995.

[10] J. A. de Zwart, P. J. Ledden, P. van Gelderen, J. Bodurka, R. Chu, and J. H. Duyn, "Signal-to-noise ratio and parallel imaging performance of a 16-channel receive-only brain coil array at 3.0 Tesla," *Magn. Reson. Med.,* vol. 51, no. 1, pp. 22 - 26, 2004.

[11] D. D. Do-Dai and R. A. Youngberg, "MRI of the hip with a shoulder surface coil in off-coronal plane," *J. Comput. Assist. Tomogr.,* vol. 19, no. 2, pp. 336 - 338, 1995.

[12] J. Doornbox, H. A. Grimbergen, P. E. Booijen, L. te Strake, J. L. Bloem, G. J. Vielvoye, and E. Boskamp, "Application of anatomically-shaped surface coils in MRI at 0.5 T.," *Magn. Reson. Med.,* vol. 3, no. 2, pp. 270-281, 1986.

[13] M. Erlichman, "Surface/specialty coil devices and gating techniques in magnetic resonance imaging," *Health Technol. Assess. Rep.,* vol. 3, pp. 1-23, 1990.

[14] A. Ettl, J. Kramer, A. Daxer, and L. Koornneef, "High resolution magnetic resonance imaging of neurovascular orbital anatomy," *Ophthalmology*, vol. 104, no. 5, pp. 869-877, 1997.

[15] T. H. Farmer, G. P. Cofer, and G. A. Johnson, "Maximizing contrast to noise with inductively coupled implanted coils," *Invest. Radiol.,* vol. 25, no. 5, pp. 552-558, 1990.

[16] S. H. Faro, S. Vinitski, H. V. Ortega, F. B. Mohamed, C. Y. Chen, A. E. Flanders, C. F. Gonzales, and R. A. Zimmerman, "Carotid magnetic resonance angiography: Improved image quality with dual 3-inch surface coils," *Neuroradiology*, vol. 38, no. 5, pp. 402-408, 1996.

[17] O. P. Gandhi and X. B. Chen, "Specific absorption rates and induced current densities for an anatomy-based model of the human for exposure to time-varying magnetic fields of MRI," *Magn. Reson. Med.,* vol. 41, no. 4, pp. 816-823, 1999.

[18] J. R. Hadley, B. E. Chapman, J. A. Roberts, D. C. Chapman, K. C. Goodrich, H. R. Buswell, A. L. Alexander, J. S. Tsuruda, and D. L. Parker, "A three-coil comparison for MR angiography," *J. Magn. Reson. Imaging,* vol. 11, no. 4, pp. 458-468, 2000.

[19] J. R. Hadley and D. L. Parker, *A Coil Coupling Model Model for Optimization Algorithms*, Toronto, Ontario, 2003.

[20] J. R. Hadley and D. L. Parker, "Relative RF coil performance in carotid imaging," *Magn. Reson. Imaging,* vol. 23, pp. 629-639, 2005.

[21] C. J. Hardy, P. A. Bottomley, K. W. Rohling, and P. B. Roemer, "An NMR phased array for human cardiac 31P spectroscopy," *Magn. Reson. Med.,* vol. 28, no. 1, pp. 54-64, 1992.

[22] C. E. Hayes, C. M. Mathis, and C. Yuan, "Surface coil phased arrays for high-resolution imaging of the carotid arteries," *J. Magn. Reson. Imaging*, vol. 6, no. 1, pp. 109-112, 1996.

[23] C. E. Hayes, J. S. Tsuruda, and C. M. Mathis, "Temporal lobes: Surface MR coil phased-array imaging," *Radiology*, vol. 189, no. 3, pp. 918-920, 1993.

[24] L. E. Hendrix, J. A. Strandt, D. L. Daniels, L. P. Mark, J. A. Borne, L. F. Czervionke, V. M. Haughton, and A. L. Williams, "Three-dimensional time-of-flight MR angiography with a surface coil: Evaluation in 12 subjects," *AJR Am. J. Roentgenol,* vol. 159, no. 1, pp. 103-106, 1992.

[25] N. Hosten and A. J. Lemke, "A special surface coil for high-resolution ocular MRI," *Front Radiat. Ther. Oncol.,* vol. 30, pp. 20-25, 1997.

[26] R. Jones, *Twelve Antenna Element Lower Extremity/Pelvic Array for MRI(A)*, Sydney, p. 440, 1998.

[27] R. Kier, R. J. Herfkens, R. A. Blinder, G. S. Leight, J. A. Utz, and P. M. Silverman, "MRI with surface coils for parathyroid tumors: Preliminary investigation," *AJR Am. J. Roentgenol.,* vol. 147, no. 3, pp. 497-500, 1986.

[28] J. H. A. Klinge, S. C. Davis, D. D. Gangahedkar, S. A. Lindsay, L. Blawat, and E. B. Boskamp, *An 8 Channel Cardiac SENSE Array*, Honolulu, p. 904, 2002.

[29] K. Y. Kojima, J. Szumowski, and R. C. Sheley, "Lower extremities: MR angiography with a unilateral telescopic phased-array coil," *Radiology*, vol. 196, pp. 871-875, 1995.

[30] M. E. Kooi, K. B. J. M Cleutjens, M. J. A. P. Daemen, P. J. E. H. M. Kitslaar, G. J. Kemerink, and J. M. A. van Engelshoven, *In-vivo and In-vitro MRI of the Carotid Artery Wall Using a Small Diameter Surface Coil*, Denver, p. 1657, 2000.

[31] J. F. Le Bas, M. Hassler, H. Reutenauer, M. Decorps, J. P. Camuset, G. Crouzet, and A. L. Benabid, "MRI of the cervical spine. Creation of a surface coil. Technical and clinical results," *J. Radiol.,* vol. 68, no. 10, pp. 579-586, 1987.

[32] A. Liffers, H. H. Quick, C. U. Herborn, H. Ermert, and M. E. Ladd, "Geometrical optimization of a phased array coil for high-resolution MR imaging of the carotid arteries," *Magn. Reson. Med*, vol. 50, no. 2, pp. 439-443, 2003.

[33] L. Malmgren, B. Geijer, S. Holtas, and F. Stahlbert, *A Two-Channel Phased Array Coil for MR-Angiography of the Extracranial Part of Carotid Artery*, Nice, p. 982, 1995.

[34] W. D. Middleton, S. Macrander, T. L. Lawson, J. B. Kneeland, J. D. Cates, G. M. Kellman, G. F. Carrera, W. D. Foley, A. Jesmanowicz, and J. S. Hyde, "High resolution surface coil magnetic resonance imaging of the joints: Anatomic correlation," *Radiographics*, vol. 7, no. 4, pp. 645-683, 1987.

[35] J. W. Monroe, P. Schmalbrock, and D. G. Spigos, "Phased array coils for upper extremity MRA," *Magn. Reson. Med.,* vol. 33, no. 2, pp. 224-229, 1995.

[36] J. R. Porter, S. M. Wright, and A. Reykowski, "A 16-element phased-array head coil," *Magn. Reson. Med.,* vol. 40, no. 2, pp. 272-279, 1998.

[37] M. Rivera, J. J. Vaquero, A. Santos, J. Ruiz-Cabello, and F. Del Pozo, "MRI visualization of small structures using improved surface coils," *Magn. Reson. Imaging*, vol. 16, no. 2, pp. 157-166, 1998.

[38] P. B. Roemer, W. A. Edelstein, C. E. Hayes, S. P. Souza, and O. M. Mueller, "The NMR phased array," *Magn. Reson. Med.,* vol. 16, no. 2, pp. 192-225, 1990.

[39] B. Roger, M. Laval-Jeantet, N. Delepine, G. Delepine, and F. Tobolski, "Magnetic resonance imaging of tumors of the knee using surface coils," *Rev. Chir. Orthop. Reparatrice Appar. Mot.,* vol. 72, no. 4, pp. 253-258, 1986.

[40] P. Schmalbrock, J. Pruski, L. Sun, A. Rao, and J. W. Monroe, "Phased array RF coils for high-resolution MRI of the inner ear and brain stem," *J. Comput. Assist. Tomogr.,* vol. 19, no. 1, pp. 8-14, 1995.

[41] M. Wiger, K. P. Pruessmann, C. Leussler, P. Roschmann, and P. Boesiger, "Specific coil design for SENSE: A six-element cardiac array," *Magn. Reson. Med.,* vol. 45, no. 3, pp. 495-504, 2001.

[42] R. M. Wilk, S. E. Harms, and L. M. Wolford, "Magnetic resonance imaging of the temporomandibular joint using a surface coil," *J. Oral Maxillofac. Surg.,* vol. 44, no. 12, pp. 935-943, 1986.

[43] M. L. Workman, M. Christensen, H. J. Griffiths and B. L. Cunningham, "Magnetic resonance imaging of the nose with surface coils: A new technique to evaluate functional and aesthetic problems," *Plast. Reconstr. Surg.,* vol. 91, no. 6, pp. 1154 - 1158, 1993.

[44] S. M. Wright and L. L. Wald, "Theory and application of array coils in MR spectroscopy," *NMR Biomed.,* vol. 10, no. 8, pp. 394 - 410, 1997.

[45] X. Zhang, K. Ugurbil, and W. Chen, "Microstrip RF surface coil design for extremely high-field MRI and spectroscopy," *Magn. Reson. Med.,* vol. 46, no. 3, pp. 443 - 450, 2001.

[46] R. A. Zimmerman, L. T. Bilaniuk, M. Yanoff, J. F. Schenck, H. R. Hart, T. H. Foster, W. A. Edelstein, P. A. Bottomley, R. W. Redington, and C. J. Hardy, "Orbital magnetic resonance imaging," *Am. J. Ophthalmol.,* vol. 100, no. 2, pp. 312-317, 1985.

[47] R. L. Haupt and S. E. Haupt, *Practical Genetic Algorithms*, John Wiley & Sons Inc., HoboKen, New Jersey, 2004.

[48] D. E. Goldbert, *Genetic Algorithms in Search, Optimization and Machine Learning*, Addison-Wesley, Reading, MA, 1989.

[49] L. Davis, *Handbook of Genetic Algorithms*, Van Nostrand Reinhold, New York, 1991.

[50] V. Cavaliere, A. Formisano, R. Martone, and M. Primizia, "A genetic algorithm approach to the design of split coil magnets for MRI," *IEEE T. Appl. Supercon,* vol. 10, no. 1, pp. 1376-1379, 2000.

[51] B. J. Fisher, N. Dillon, T. A. Carpenter, and L. D. Hall, "Design of a biplanar gradient coil using a genetic algorithm," *Magn. Reson. Imaging,* vol. 15, no. 3, pp. 369-376, 1997.

[52] D. Yau and S. Crozier, "A genetic algorithm/ method of moments approach to the optimization of an RF coil for MRI applications – theoretical considerations," *PIER (Progress in Electromagnetics Research),* vol. 39, pp. 177-192, 2003.

[53] P. Andris and I. Frollo, "Optimizationof NMR coils by genetic algorithms," *Measurement Science Review,* vol. 2, sec. 2, pp. 13-22, 2002.

[54] B. J. Fisher, N. Dillon, T. A. Carpenter, and L. D. Hall, "Design by genetic algorithm of a z gradient set for magnetic resonance imaging of the human brain," *Measurement Science and Technology,* vol. 6, pp. 904-909, 1995.

[55] N. Lu, J. Jin, E. Michielssen, and R. L. Magin, *Optimization of RF Coil Design Using Genetic*

Algorithm and Simulated Annealing Method, Nice, p. 1002, 1995.

[56] W. R. Smythe, *Static and Dynamic Electricity*, McGraw-Hill Book Company, New York, pp. 290-291, 1968.

[57] M. Misakian, "Equations for the magnetic field produced by one or more rectangular loops of wire in the same plane," *J. Res. Natl. Inst. Stan.,* vol. 105, no. 4, pp. 557-564, 2000.

[58] D. I. Hoult, "The principle of reciprocity in signal strength calculations – A mathematical guide," *Concepts in Magnetic Resonance*, vol. 12, no. 4, pp. 173-187, 2000.

[59] W. L. Stutzman and G. A. Thiele, *Antenna Theory and Design*, John Wiley & Sons Inc., New York, pp. 102-103, 1981.

[60] F. W. Grover, *Inductance Calculations: Working Formulas and Tables,* D. Van Nostrand Company Inc., New York, 1946.

[61] C. E. Hayes, N. Hattes, and P. B. Roemer, "Volume imaging with MR phased arrays," *Magn. Reson. Med,* vol. 18, no. 2, pp. 309-319, 1991.

[62] C. E. Hayes and P. B. Roemer, "Noise correlations in data simultaneously acquired from multiple surface coil arrays," *Magn. Reson. Med.,* vol. 16, no. 2, pp. 181-191, 1990.

[63] E. B. Boskamp, L. Blawat, K. F. King, J. Lorbiecki, and A. B. Tiwari, *A 16-Channel Neurovascular SENSE Array,* Honolulu, p. 852, 2002.

[64] D. J. Weyers and E. B. Boskamp, *An 8-Channel Volume RF Transmit Coil*, Honolulu, p. 901, 2002.

[65] R. F. Lee, R. O. Giaquinto, and C. J. Hardy, "Coupling and decoupling theory and its application to the MRI phased array," *Magn. Reson. Med.,* vol. 48, pp. 203-213, 2002.

[66] K. P. McGee, J. P. Debbins, E. B. Boskamp, L. Blawat, L. Angelos, and K. F. King, "Cardiac magnetic resonance parallel imaging at 3.0 Tesla: Technical feasibility and advantages," *J. Magn. Reson. Imaging*a, vol. 19, no. 3, pp. 291-297, 2004.

[67] G. R. Duensing, H. R. Brooker, and J. R. Fitzsimmons, "Maximizing signal-to-noise ratio in the presence of coil coupling," *J. Magn. Reson. B.,* vol. 111, no. 3, pp. 230-235.

[68] F. A. Breuer, M. Blaimer, M. F. Mueller, R. M. Heidemann, M. A. Griswold, and P. M. Jakob, *Finding the Optimal Sampling Pattern in 2D Parallel Imaging for a Given Receiver Coil Configuration,* Miami, Florida, Morning categorical course, 2005.

[69] M. A. Griswold, *RF Coils for Parallel Imaging*, Miami, Florida, Morning categorical course, 2005.

[70] N. Famili, S. M. Wright, and J. R. Porter, "MR flow measurement using RF phase gradients in receiver coil arrays," *IEEE Trans. Biomed. Eng.,* vol. 40, no. 12, pp. 1243-1249, 1993.

[71] S. M. Wright, R. L. Magin, and J. R. Kelton, "Arrays of mutually-coupled receiver coils: theory and application," *Magn. Reson. Med.,* vol. 17, no. 1, pp. 252-268, 1991.

[72] R. Pascone, T. Vullo, J. Farrelly, and P. T. Cahill, "Explicit treatment of mutual inductance in eight-solumn birdcage resonators," *Magn. Reson. Imaging*, vol. 10, no. 3, pp. 401-410, 1992.

[73] R. J. Pascone, B. J. Garcia, T. M. Fitzgerald, T. Vullo, R. Zipagan, and P. T. Cahill, "Generalized electrical analysis of low-pass and high-pass birdcage resonators," *Magn. Reson. Imaging*, vol. 9, no. 3, pp. 395-408, 1991.

[74] R. Pascone, T. Vullo, J. Farrelly, R. Mancuso, and P. T. Cahill, "Use of transmission line analysis for multi-tuning of birdcage resonators," *Magn. Reson. Imaging,* vol. 11, no. 5, pp. 705-715, 1993.

[75] T. J. Lawry, M. W. Weiner, and G. B. Matson, "Computer modeling of surface coil sensitivity," *Magn. Reson. Med.,* vol. 16, no. 2, pp. 294-302, 1990.

[76] J. Jin, G. Shen, and T. Perkins, "On the field inhomogeneity of a birdcage coil," *Magn. Reson. Med.,* vol. 32, no. 3, pp. 418-422, 1994.

[77] J. Jin, *Electromagnetic Analysis and Design in Magnetic Resonance Imaging,* CRC Press, Boca Raton, Florida, 1999.

[78] T. Vullo, R. Pascone, R. Mancuso, R. Zipagan, and P. T. Cahill, "Transmission line analysis of noncylindrical birdcage resonators," *Magn. Reson. Imaging,* vol. 12, no. 5, pp. 785-797, 1994.

[79] J. R. Hadley, *Design of Optimal Radio Frequency Coil Arrays for Magnetic Resonance Angiography*, Ph.D. Dissertation, Department of Electrical and Computer Engineering, University of Utah, Salt Lake City, UT, 2005.